RSC Advances

ROYAL SOCIETY OF CHEMISTRY

PAPER

View Article Online
View Journal | View Issue

Cite this: *RSC Adv.*, 2020, **10**, 14525

Excitation dependent visible and NIR photoluminescence properties of Er^{3+}, Yb^{3+} co-doped $NaBi(MoO_4)_2$ nanomaterials†

Pushpendra, Ravi K. Kunchala, Rimple Kalia and Boddu S. Naidu *

Received 10th February 2020
Accepted 30th March 2020

DOI: 10.1039/d0ra01272f

rsc.li/rsc-advances

Due to the exceptional luminescence properties of lanthanide doped nanomaterials, they have applications in various field such as sensing, photocatalysis, solar cells, bio-imaging, therapy, diagnostics, anti-counterfeiting, latent fingerprint development, optical amplifiers, solid state lighting, *etc.* Here, we report the excitation dependent photoluminescence properties of Yb^{3+}, Er^{3+} co-doped $NaBi(MoO_4)_2$ nanomaterials in both the visible and NIR regions upon UV, visible and NIR excitation. These photoluminescence properties show that strong energy transfer occurs from the host to the Yb^{3+}, Er^{3+} ions. These materials show major emission bands at 530, 552 (green) and 656 nm (red) in the visible region and 1000 and 1534 nm in the NIR region. The intensity ratio between green and red bands is dependent on the excitation wavelength, whereas the intensity ratio of the 1000 and 1534 nm bands relies on the excitation wavelength and Er^{3+} doping concentration. These materials also exhibit host emission and upconversion luminescence properties in the visible region.

1. Introduction

Lanthanide ions are known to have excellent luminescence properties in the UV, visible and NIR regions due to their rich energy levels. These ions also show both down-shifting and upconversion photoluminescence properties with long excited state lifetime values and high quantum yields.[1,2] Due to these exceptional luminescence properties, lanthanide doped nanomaterials have applications in various fields such as sensing, photocatalysis, solar cells, bio-imaging, therapy, diagnostics, anti-counterfeiting, latent fingerprint development, optical amplifiers, solid state lighting, *etc.*[1–8] Among lanthanide ions, the trivalent erbium ion shows emission in the visible and NIR regions and also exhibits upconversion luminescence properties. However, its upconversion luminescence properties are very poor if it is doped alone due to low absorption cross section. To improve the upconversion luminescence properties, Yb^{3+} is used as a sensitizer, where it absorbs the NIR radiation and transfer the energy to the Er^{3+} ion. Energy transfer from Yb^{3+} to Er^{3+} and Er^{3+} to Er^{3+} are also investigated in detail.[9,10] Among the lanthanide ions, Yb^{3+}, Er^{3+} doped upconversion materials are well known for their unique optical features, such as excellent upconversion luminescence, long excited state lifetime, and high quenching concentration compared to other rare earth ions.[11,12] Recently, Yb^{3+}, Er^{3+} co-doped dual mode emitting materials become key players in anti-counterfeiting technology due to their unique luminescence properties under both UV and NIR illuminations.[13–16]

However, most of these host materials are rare earth based fluorides. These materials are toxic, very expensive and getting large quantity of high purity rare earth materials is very difficult. Recently, reports on lanthanide doped bismuth based nanomaterials are increasing gradually due to its advantages over rare earths such as nontoxic nature, more abundant, less expensive and an environment ecofriendly, which could be termed as 'Green Bismuth'.[17–27] Also, ionic size, charge, coordination number of bismuth is similar to rare earth ions. Bismuth activated materials are known to have their characteristic emission properties which makes them more important class of luminescent materials.[28–30] $NaBi(MoO_4)_2$ is an excellent host material for lanthanide ions with excellent luminescence properties. For example, Gan, *et al.* reported the luminescence properties of Eu^{3+}, Gd^{3+} co-doped $NaBi(MoO_4)_2$ materials.[22] Rico, *et al.* studied upconversion luminescence properties of Er^{3+} doped single crystals.[26] Li, *et al.* reported white light emission from Eu^{3+}, Dy^{3+} co-doped $NaBi(MoO_4)_2$ materials and their use in light emitting diode.[23] Li and Deun investigated upconversion properties of Er^{3+}/Yb^{3+} co-doped bulk materials.[27] Very recently, our group has been reported the room temperature synthesis of Eu^{3+} doped $NaBi(MoO_4)_2$ nanomaterials and their luminescence properties.[24] In the present manuscript, we are reporting visible and NIR photoluminescence of $NaBi_{0.9-x}Er_xYb_{0.1}(MoO_4)_2$ nanomaterials upon UV, visible and NIR excitations. To the best of authors knowledge, so far there is no

Institute of Nano Science and Technology (INST), Phase 10, Sector 64, Mohali, Punjab, India-160062. E-mail: naidu245@gmail.com; sanyasinaidu@inst.ac.in

† Electronic supplementary information (ESI) available: Details of synthesis and characterization techniques, FTIR and Raman Spectra, XRD patterns, PL spectra of as synthesized nanomaterials. See DOI: 10.1039/d0ra01272f

report on visible, NIR and upconversion luminescence properties of $NaBi_{0.9-x}Er_xYb_{0.1}(MoO_4)_2$ nanomaterials.

2. Results and discussion

Nanomaterials of $NaBi_{0.9-x}Er_xYb_{0.1}(MoO_4)_2$, $(0.01 \leq x \leq 0.1)$ are prepared by co-precipitation method at room temperature. The detailed synthesis procedure and characterization techniques details are given in ESI.† X-ray diffraction patterns of $NaBi_{0.9-x}Er_xYb_{0.1}(MoO_4)_2$, $(0.01 \leq x \leq 0.1)$ nanomaterials (Fig. S1, ESI†) shows that all doped materials crystallized in scheelite structure. They match completely with the standard JCPDS file # 01-074-8694 of $NaBi(MoO_4)_2$. Crystallite size of all these nanomaterials is calculated using Debye–Scherrer formula and is found to be 13 nm for all samples. Raman and FTIR spectra of all doped samples (Fig. S2 and S3, ESI†) are similar to that of undoped sample as well as reported data.[31,32] Absence of extra peak confirm that there is no amorphous impurity phase present in these materials. DR UV-vis spectra shows that Er^{3+} absorption increases with its concentration (Fig. S4, ESI†). TEM image of these nanomaterials shows that they consist of nearly spherical particles with size in the range of 5–18 nm (Fig. S5, ESI†). EDS analysis of these materials shows that the actual composition of metal ions is similar to the added composition (Fig. S6, ESI†).

Luminescence properties of $NaBi_{0.9-x}Er_xYb_{0.1}(MoO_4)_2$, $(0.01 \leq x \leq 0.1)$ nanomaterials in visible region are recorded at 488 nm excitation and shown in Fig. 1(a). Three major transitions corresponding to $^2H_{11/2} \rightarrow {}^4I_{15/2}$ (530 nm, green), $^4S_{3/2} \rightarrow {}^4I_{15/2}$ (552 nm, green) and $^4F_{9/2} \rightarrow {}^4I_{15/2}$ (656 nm, red) of Er^{3+} are observed. Intensity of these transitions increases with the concentration of Er^{3+} till $x = 0.05$ and thereafter it started decreasing. The initial increase in the intensity with Er^{3+} concentration is due to increase in the number of Er^{3+} ions getting excited. However, with further increase in Er^{3+} concentration, Er–Er cross-relaxation and multi phonon relaxation leads to non-radiative decay. Hence, $x = 0.05$ of Er^{3+} is an optimum concentration for obtaining maximum photoluminescence in this host material. Excitation spectra corresponding to Er^{3+} emission (552 nm) of these nanomaterials are shown in Fig. 1(b). It consists of very broad band between 250–370 nm corresponding to host material (combination of molybdate charge transfer and s–p transition of Bi^{3+}) and few sharp peaks corresponding to f–f transition of Er^{3+} ions. Intensity of all these transitions increases with the concentration of Er^{3+} till 0.05 and thereafter it decreases. The observation of host absorption while monitoring Er^{3+} emission confirm the transfer of energy from host to Er^{3+}. There is another broad band between 400–500 nm corresponding to some trap states present in the host materials and its intensity continuously decrease with increase in the Er^{3+} concentration.

Emission spectra of these materials are recorded by exciting host material (290, 335 nm) as well as direct Er^{3+} ions (452, 488, 522 nm) for better understanding of the interaction between host material and dopant ions. Emission spectra of $NaBi_{0.85}Er_{0.05}Yb_{0.1}(MoO_4)_2$ nanomaterials excited at different

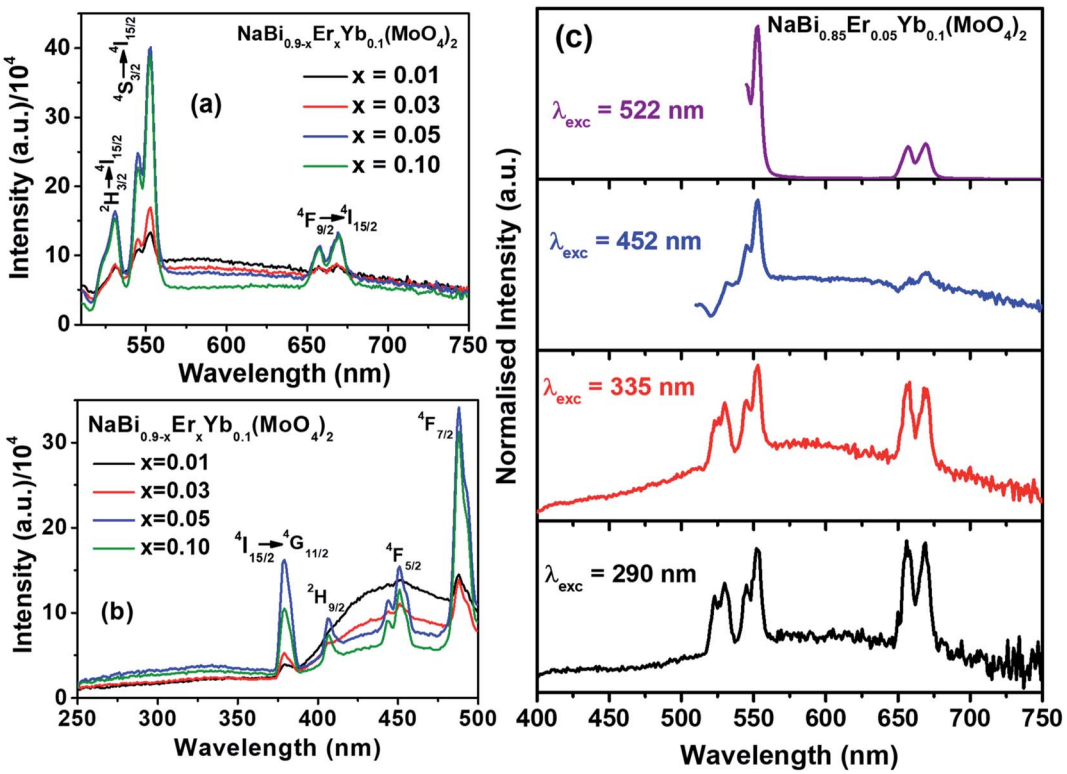

Fig. 1 (a) Emission spectra excited at 488 nm, (b) excitation spectra monitored at 552 nm emission of $NaBi_{0.9-x}Er_xYb_{0.1}(MoO_4)_2$, $(0.01 \leq x \leq 0.1)$ nanomaterials. (c) Emission spectra of $NaBi_{0.85}Er_{0.05}Yb_{0.1}(MoO_4)_2$ nanomaterials excited at 290, 335, 452, 522 nm.

wavelength are shown in Fig. 1(c). Emission spectra obtained by exciting host material (290, 335 nm) exhibit nearly equal intensities of green and red emission peaks with broad background emission centered around 570 nm. This broad emission is due to the trap states present in the host material. In case of direct excitation of Er^{3+}, the material emit strong green and week red light. These results demonstrate that equal energy transfer from host material to $^2H_{11/2}$, $^4S_{3/2}$, and $^4F_{9/2}$ levels of Er^{3+} occurs. Whereas $^2H_{11/2}$, $^4S_{3/2}$ levels are more populated than $^4F_{9/2}$ level after direct excitation of Er^{3+} ions. Similar kind of results are observed in all Er^{3+} and Yb^{3+} co-doped samples (Fig. S7–S9,† ESI).

Emission spectra in near infrared (NIR) region of $NaBi_{0.9-x}Er_xYb_{0.1}(MoO_4)_2$, $(0.01 \leq x \leq 0.1)$ nanomaterials are recorded at 522 nm excitation and presented in Fig. 2(a). It consists of two emission bands, *i.e.*, one weak band corresponding to $^4I_{11/2} \rightarrow {}^4I_{15/2}$ (1000 nm) and a strong band with fine splitting due to $^4I_{13/2} \rightarrow {}^4I_{15/2}$ (1534 nm) transitions of Er^{3+}. Their intensity increases with the concentration of Er^{3+} till 0.05, thereafter decreases. The reduction in the intensity of emission above $x = 0.05$ is assigned to the concentration quenching. Similar kind of trend is also observed for Er^{3+} emission in the literature.[33,34] Excitation spectra of $NaBi_{0.9-x}Er_xYb_{0.1}(MoO_4)_2$, $(0.01 \leq x \leq 0.1)$ nanomaterials are monitored at 1534 nm emission and shown in Fig. 2(b). A broad band centered at 290 nm along with several sharp peaks are observed. The former is assigned to host materials absorption and later ones are corresponding to f–f transitions of Er^{3+} in the host matrix. The observation of host absorption while monitoring 1534 nm emission reveals the energy transfer from host to Er^{3+} ion. However, the lower intensity of host absorption suggest that the energy transferred to the Er^{3+} leads to several f–f transitions in visible and NIR regions.

To understand the energy transfer from $NaBi(MoO_4)_2$ to Er^{3+}, Yb^{3+} ions, emission spectra of these nanomaterials in NIR region are recorded at 290 nm and shown in Fig. 2(c). All these spectra have bands at 1000, 1534 nm. The 1000 nm band corresponding to the combination of $^4I_{11/2} \rightarrow {}^4I_{15/2}$, $^2F_{5/2} \rightarrow {}^2F_{7/2}$ transitions of Er^{3+}, Yb^{3+} ions, respectively and the 1534 nm band is due to $^4I_{13/2} \rightarrow {}^4I_{15/2}$ transition of Er^{3+}. Surprisingly, the emission intensity of 1000 nm band is much higher when compared to the 1534 nm band and the intensity of former band decreases with increasing the Er^{3+} concentration whereas the intensity of later increases. However, the rate at which former decrease is very high while the increment in later is marginal. It can be explained based on two things. First one is the competitive energy transfer from host to Yb^{3+} and Er^{3+} simultaneously. Second, the energy transferred from host to the Yb^{3+} leads to emission at 1000 nm only whereas it is distributed in different 'f' energy levels of Er^{3+} and gives several emission bands at 530, 552, 656, 890, 1000 and 1534 nm. Excitation spectra are monitored at 1000 nm emission for these nanomaterials and shown in Fig. 2(d). These spectra consists of strong excitation band at 290 nm with shoulder at 380 nm and very week peaks at 522, 656 nm. The broad band is ascribed to host absorption and its intensity decreases with increase in the Er^{3+} concentration. This might be because of the competitive energy transfer from host to the Yb^{3+} and Er^{3+} ions. Contour plots of emission and excitation for $NaBi_{0.85}Er_{0.05}Yb_{0.1}(MoO_4)_2$ nanomaterials are shown in the Fig. 3. It gives possible

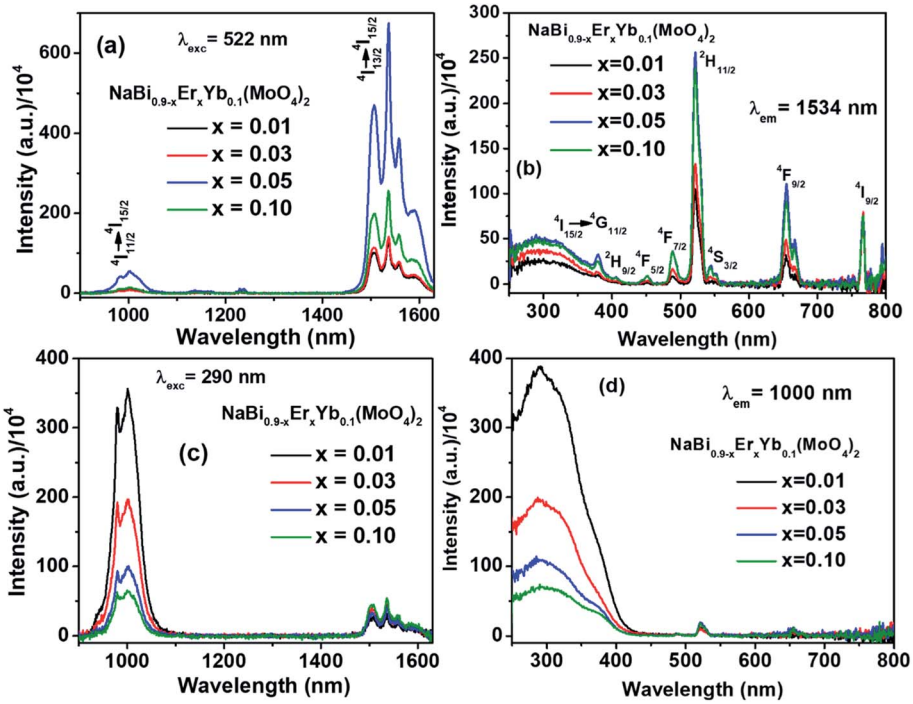

Fig. 2 Emission spectra excited at (a) 522 nm, (c) 290 nm and excitation spectra monitored at (b) 1534 nm, (d) 1000 nm emission of $NaBi_{0.9-x}Er_xYb_{0.1}(MoO_4)_2$, $(0.01 \leq x \leq 0.1)$ nanomaterials.

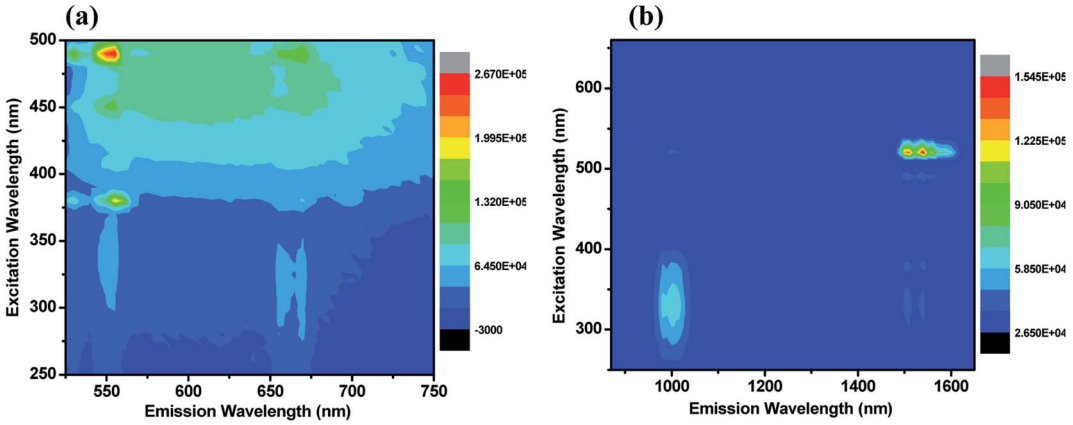

Fig. 3 Contour plot of emission–excitation of $NaBi_{0.85}Er_{0.05}Yb_{0.1}(MoO_4)_2$ nanomaterials for corresponding emission in the (a) visible, (b) NIR regions.

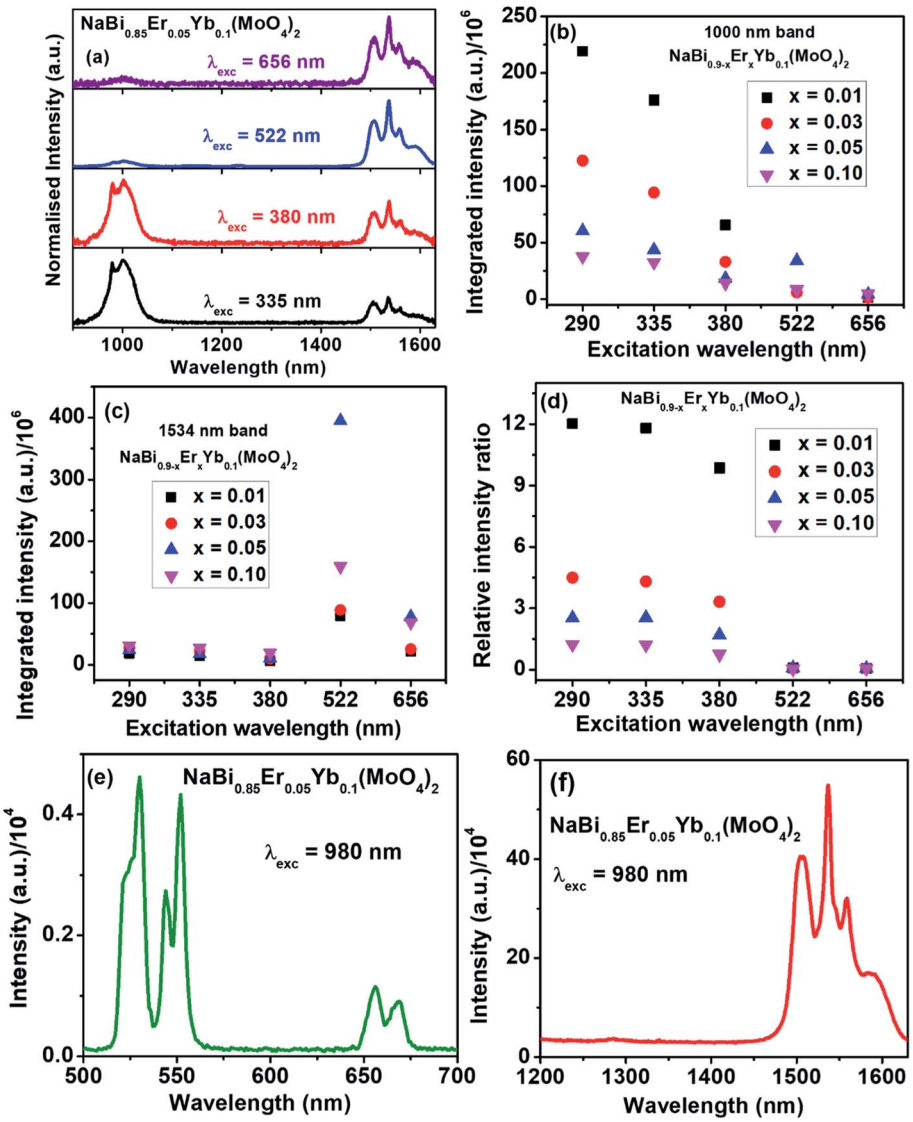

Fig. 4 (a) Emission spectra of $NaBi_{0.85}Er_{0.05}Yb_{0.1}(MoO_4)_2$ nanomaterials excited at 335, 380, 522, 656 nm. Integrated intensities of (b) 1000 nm peak, (c) 1534 nm peak, (d) ratio of 1000/1534 nm peaks for $NaBi_{0.9-x}Er_xYb_{0.1}(MoO_4)_2$, ($0.01 \leq x \leq 0.1$) nanomaterials at different excitations. Emission spectra of $NaBi_{0.85}Er_{0.05}Yb_{0.1}(MoO_4)_2$ nanomaterials excited at 980 nm in (e) visible (f) NIR regions.

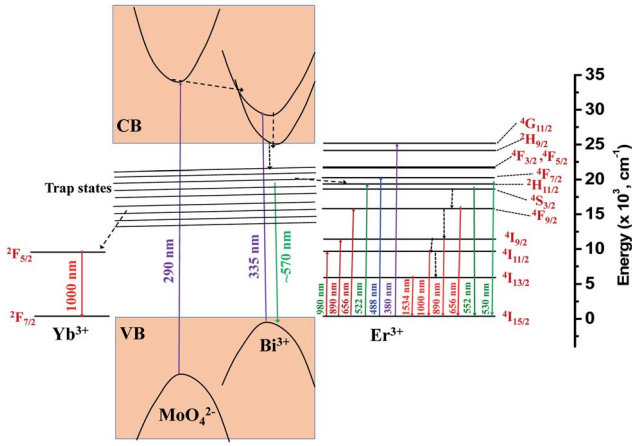

Fig. 5 Energy level diagram of $NaBi_{0.9-x}Er_xYb_{0.1}(MoO_4)_2$ nanomaterials and possible energy transitions.

excitation wavelengths and corresponding emission intensities in a qualitative way. It shows that the relative emission intensities in the NIR region are highly dependent on the excitation wavelength.

For better quantitative understanding of NIR emission properties, $NaBi_{0.85}Er_{0.05}Yb_{0.1}(MoO_4)_2$ nanomaterials are excited through host (335, 380 nm) as well as Er^{3+} ions (522, 656 nm) directly and results are shown in Fig. 4(a). When the sample excited directly to Er^{3+} ion (522, 656 nm), very strong emission at 1534 nm and weak band at 1000 nm are observed. However, the trend is just reversed when excited to host material. It reveals that the Er^{3+} ion has very low contribution to the 1000 nm emission and the emission is majorly resulted from $^2F_{5/2} \rightarrow {}^2F_{7/2}$ transition of Yb^{3+} ions. Similar results are also observed from all $NaBi_{0.9-x}Er_xYb_{0.1}(MoO_4)_2$, $(0.01 \leq x \leq 0.1)$ nanomaterials (Fig. S10–S12, ESI†). Integrated area of 1000, 1534 nm bands and their relative intensity ratios are measured for all these samples at different excitation wavelengths (Table TS2, ESI†) and corresponding plots are shown in Fig. 4(b–d). The ratio of 1000 nm band to 1534 nm band is maximum for samples excited at 290 nm followed by 335, 380 nm and is least for 522 nm excitation. The ratio decreases with increasing the Er^{3+} concentration in the host matrix. As Yb^{3+} is a good sensitizer for upconversion luminescence properties, to know the possibility of the upconversion emission from these samples, $NaBi_{0.85}Yb_{0.1}Er_{0.05}(MoO_4)_2$ nanomaterials are excited with 980 nm laser light having 2.75 W cm^{-2} power density at room temperature and emission is recorded in the range of 500–750 nm. The emission spectrum is shown in Fig. 4(e). This material shows excellent upconversion properties with emission peaks at 530, 552, 656 nm. These bands are corresponding to $^2H_{11/2} \rightarrow {}^4I_{15/2}$ (530 nm), $^4S_{3/2} \rightarrow {}^4I_{15/2}$ (552 nm) and $^4F_{9/2} \rightarrow {}^4I_{15/2}$ (656 nm) transition of Er^{3+} ion. Emission properties are also measured in the NIR region at 980 nm laser excitation and is shown in Fig. 4(f). The sample gives very strong emission at 1534 nm. It reveals that only part of the 980 nm laser light is converted into upconversion emission and remaining energy converted into NIR emission while decay to ground state.

Based on the photoluminescence properties observed in visible, NIR regions, a possible energy level diagram for $NaBi_{0.9-x}Er_xYb_{0.1}(MoO_4)_2$ nanomaterials is proposed as illustrated in the Fig. 5. When the host material is excited, it decays non-radiatively to the trap states present in it. From there it may decay radiatively to the valence band by emitting very broad emission centered at 570 nm or it may transfer its energy to Yb^{3+} and Er^{3+} ions. In case of energy transfer from host to the Yb^{3+} ions, they decay to ground state by emitting 1000 nm emission. In the event of the energy transfer to Er^{3+} ions, part of these ions decay to ground state by giving visible emission and part of the ions decay non-radiatively to lower energy levels and subsequently they decay to the ground state by emitting NIR light. If these nanomaterials are excited directly to Er^{3+}, they give only Er^{3+} emission.

3. Conclusions

Nanomaterials of $NaBi_{0.9-x}Er_xYb_{0.1}(MoO_4)_2$ exhibit excellent photoluminescence properties in both visible and NIR regions by exciting with UV, visible and NIR light. These nanomaterials show broad emission in visible region by exciting host material along with Er^{3+} emission. Strong energy transfer from host to Er^{3+}, Yb^{3+} and Yb^{3+} to Er^{3+} has been observed. The luminescence properties of these nanomaterials depends on the excitation wavelength. The relative intensity ratio between green to red emission and 1000 nm to 1534 nm emission peaks are highly depend on the direct or indirect excitation of Er^{3+} ions. The broad host emission in visible region and excitation dependent difference in relative intensities of emission peaks shows that these nanomaterials may have potential applications in anti-counterfeiting ink as security labels.

Conflicts of interest

There are no conflicts to declare.

Acknowledgements

P, RKK and RK are grateful to INST, Mohali for the fellowship. BSN acknowledges the DST-SERB, India (File number: ECR/2015/000333) for financial assistance.

References

1 G. Blasse and B. C. Grabmaier, *Luminescent Materials*, Springer-Verlag Berlin Heidelberg, 1994.
2 S. Wen, J. Zhou, K. Zheng, A. Bednarkiewicz, X. Liu and D. Jin, *Nat. Commun.*, 2018, **9**, 2415.
3 Y. Hu, Q. Shao, X. Deng, D. Song, S. Han, Y. Dong and J. Jiang, *J. Mater. Chem. C*, 2019, **7**, 11770–11775.
4 J. Zhou, Q. Liu, W. Feng, Y. Sun and F. Li, *Chem. Rev.*, 2015, **115**, 395–465.
5 J. Zhao, J. Gao, W. Xue, Z. Di, H. Xing, Y. Lu and L. Li, *J. Am. Chem. Soc.*, 2018, **140**, 578–581.
6 E. Downing, L. Hesselink, J. Ralston and R. Macfarlane, *Science*, 1996, **273**, 1185–1189.

7 F. Vetrone, R. Naccache, A. Zamarrón, A. J. De La Fuente, F. Sanz-Rodríguez, L. M. Maestro, E. M. Rodriguez, D. Jaque, J. G. Sole and J. A. Capobianco, *ACS Nano*, 2010, **4**, 3254–3258.
8 Z. Gu, L. Yan, G. Tian, S. Li, Z. Chai and Y. Zhao, *Adv. Mater.*, 2013, **25**, 3758–3779.
9 M. T. Berry and P. S. May, *J. Phys. Chem. A*, 2015, **119**, 9805–9811.
10 A. Baride, P. S. May Jr and M. T. Berry, *J. Phys. Chem. C*, 2020, **124**, 2193–2201.
11 F. Auzel, *Chem. Rev.*, 2004, **104**, 139–173.
12 M. Haase and H. Schäfer, *Angew. Chem., Int. Ed.*, 2011, **50**, 5808–5829.
13 J. Andres, R. D. Hersch, J.-E. Moser and A.-S. Chauvin, *Adv. Funct. Mater.*, 2014, **24**, 5029–5036.
14 W. Yao, Q. Tian, J. Liu, Z. Wu, S. Cui, J. Ding, Z. Daia and W. Wu, *J. Mater. Chem. C*, 2016, **4**, 6327–6335.
15 Y. Zhang, L. Zhang, R. Deng, J. Tian, Y. Zong, D. Jin and X. Liu, *J. Am. Chem. Soc.*, 2014, **136**, 4893–4896.
16 J. Liu, H. Rijckaert, M. Zeng, K. Haustraete, B. Laforce, L. Vincze, I. V. Driessche, A. M. Kaczmarek and R. V. Deun, *Adv. Funct. Mater.*, 2018, **28**, 1707365.
17 R. Mohan, *Nat. Chem.*, 2010, **2**, 336.
18 M. Back, E. Trave, N. Mazzucco, P. Riello and A. Benedetti, *Nanoscale*, 2017, **9**, 6353–6361.
19 P. Lei, R. An, S. Yao, Q. Wang, L. Dong, X. Xu, K. Du, J. Feng and H. Zhang, *Adv. Mater.*, 2017, **29**, 1700505.
20 B. S. Naidu, B. Vishwanadh, V. Sudarsan and R. K. Vatsa, *Dalton Trans.*, 2012, **41**, 3194–3203.
21 S. Sarkar, A. Dash and V. Mahalingam, *Chem.–Asian J.*, 2013, **9**, 447–451.
22 Y. Gan, W. Liu, W. Zhang, W. Li, Y. Huang and K. Qiu, *J. Alloys Compd.*, 2019, **784**, 1003–1010.
23 W. Li, W. Zhang, W. Li, Y. Gan and P. Zhang, *J. Mater. Sci.: Mater. Electron.*, 2019, **30**, 658–666.
24 Pushpendra, R. K. Kunchala, S. N. Achary, A. K. Tyagi and B. S. Naidu, *Cryst. Growth Des.*, 2019, **19**, 3379–3388.
25 Pushpendra, R. K. Kunchala, S. N. Achary and B. S. Naidu, *ACS Appl. Nano Mater.*, 2019, **2**, 5527–5537.
26 M. Rico, V. Volkov and C. Zaldo, *J. Alloys Compd.*, 2001, **323–324**, 806–810.
27 K. Li and R. V. Deun, *Inorg. Chem.*, 2019, **58**, 6821–6831.
28 J. Cao, L. Li, L. Wang, X. Li, Z. Zhang, S. Xu and M. Peng, *J. Mater. Chem. C*, 2018, **6**, 5384–5390.
29 J. Cao, L. Wondraczek, Y. Wang, L. Wang, J. Li, S. Xu and M. Peng, *ACS Photonics*, 2018, **5**, 4393–4401.
30 J. Cao, S. Xu, Q. Zhang, Z. Yang and M. Peng, *Adv. Opt. Mater.*, 2018, **6**, 1801059.
31 J. Hanuza and M. Maczka, *Vib. Spectrosc.*, 1994, **7**, 85–96.
32 J. Hanuza, A. Haznar, M. Maczka, A. Pietraszko, A. Lemiec, J. H. van der Maas and E. T. G. Lutz, *J. Raman Spectrosc.*, 1997, **28**, 953–963.
33 L. Li, X. Zhang, Z. Bai, W. Dong, H. Shi and Q. Xue, *Infrared Phys. Technol.*, 2015, **73**, 49–53.
34 V. R. Prasad, B. Haritha, S. Damodaraiah and Y. C. Ratnakaram, *Infrared Phys. Technol.*, 2018, **94**, 184–190.

